Research Square

Preprints are preliminary reports that have not undergone peer review.
They should not be considered conclusive, used to inform clinical practice,
or referenced by the media as validated information.

Biomechanical performance and posterior exposure demand of a cortical bone trajectory–reverse cortical bone trajectory hybrid construct in transforaminal lumbar interbody fusion under osteoporotic conditions: a finite element analysis

Zhihao Kang
Qilu Hospital of Shandong University
Xinlong Lu
Qilu Hospital of Shandong University
Haipeng Si
Qilu Hospital (Qingdao) of Shandong University
Kaibin Wang
Qilu Hospital of Shandong University
Xu Zhai
Qilu Hospital of Shandong University
Xichao Wang
Qilu Hospital of Shandong University
Yanpeng Feng
Qilu Hospital of Shandong University
Xinyang Guo
Qilu Hospital of Shandong University
Chen Liu
Qilu Hospital of Shandong University
Wencan Zhang
Qilu Hospital of Shandong University
Le Li
Qilu Hospital of Shandong University
Wanlong Xu
xuwanlong20082008@163.com
Qilu Hospital of Shandong University

Research Article

Keywords: Reverse cortical bone trajectory, Cortical bone trajectory, Osteoporosis, Transforaminal lumbar interbody fusion, Finite element analysis

Posted Date: November 18th, 2026

DOI: https://doi.org/10.21203/rs.3.rs-11338505/v1

License: This work is licensed under a Creative Commons Attribution 4.0 International License. Read Full License

Additional Declarations: No competing interests reported.

Biomechanical performance and posterior exposure demand of a cortical bone trajectory–reverse cortical bone trajectory hybrid construct in transforaminal lumbar interbody fusion under osteoporotic conditions: a finite element analysis

Zhihao Kang[a,#], Xinlong Lu[a,#], Haipeng Si[a,b,#], Kaibin Wang[a], Xu Zhai[a], Xichao Wang[a], Yanpeng Feng[a], Xinyang Guo[a], Chen Liu[a], Wencan Zhang[a], Le Li[a], Wanlong Xu[a*].

[a] Department of Orthopedics, Qilu Hospital of Shandong University, Cheeloo College of Medicine, Shandong University, Jinan 250012, Shandong, China.

[b] Key Laboratory of Qingdao in Medicine and Engineering, Department of Orthopedics, Qilu Hospital (Qingdao) of Shandong University, Qingdao 266035, Shandong, China.

[#] These authors contributed equally to this work and should be considered co-first authors.

[*] Corresponding author at: Department of Orthopedics, Qilu Hospital of Shandong University, Cheeloo College of Medicine, Shandong University, Jinan 250012, Shandong, China. Email: xuwanlong20082008@163.com

Abstract

Background: In osteoporotic patients undergoing transforaminal lumbar interbody fusion (TLIF), achieving sufficient segmental stability while reducing posterior surgical exposure remains challenging. This finite element study aimed to evaluate whether a cortical bone trajectory–reverse cortical bone trajectory (CBT–RCBT) hybrid construct could balance fixation stability and posterior exposure requirements in osteoporotic TLIF.

Methods: A validated three-dimensional finite element (FE) model of the lumbosacral spine (L3–S1) was developed from thin-slice computed tomography data. An L4–L5 TLIF model was created, and three posterior fixation constructs were simulated under both normal and osteoporotic bone conditions: traditional-trajectory pedicle screws (TT–TT), cortical bone trajectory screws (CBT–CBT), and a hybrid construct combining cranially directed CBT with caudally directed reverse CBT (CBT–RCBT). The inferior surface of S1 was fully constrained. A 500-N compressive follower load and a superimposed 10 N·m moment were applied to simulate flexion, extension, lateral bending, and axial rotation. Outcome measures included L4–L5 range of motion (ROM), interbody cage stress, posterior screw–rod peak stress, mean adjacent-disc stress, and normalized posterior exposure area.

Results: Under osteoporotic conditions, the CBT–RCBT construct yielded lower ROM than TT–TT and CBT–CBT in extension (0.4195°), lateral bending (0.8978°), and axial rotation (0.4268°), whereas flexion ROM was not the lowest (0.8604°). Compared with CBT–CBT, CBT–RCBT reduced peak stress in the screw–rod system by 17.37%–

52.77%, with rotational loading decreasing from 302.1203 MPa to 142.6792 MPa. Cage stress under extension, lateral bending, and axial rotation was also reduced (7.8800 vs 8.0800 MPa; 27.3700 vs 29.7250 MPa; 21.8500 vs 24.9350 MPa), while mean adjacent-disc stress showed no consistent increase across constructs. The normalized posterior exposure area was lowest for the CBT–RCBT strategy (TT–TT:CBT–CBT:CBT–RCBT = 1 : 0.6988 : 0.4038).

Conclusions: In this osteoporotic TLIF finite element model, the CBT‑RCBT hybrid construct demonstrated a direction-dependent biomechanical advantage, with improved stability in extension, lateral bending, and axial rotation, lower posterior fixation stress than CBT‑CBT, and reduced posterior exposure demand. These findings support further biomechanical and clinical evaluation of CBT‑RCBT in osteoporotic TLIF when reduced posterior exposure is desirable.

Keywords: Reverse cortical bone trajectory; Cortical bone trajectory; Osteoporosis; Transforaminal lumbar interbody fusion; Finite element analysis

Background

Lumbar fusion is a cornerstone procedure for degenerative disease, instability, and traumatic injury, and its long-term effectiveness largely depends on whether posterior fixation can provide reliable stability [1–3]. With population aging, osteoporosis has become a key determinant of construct stability and complication risk in fusion surgery [4,5]. Among patients older than 50 years undergoing spine surgery, 46.1% of men have osteopenia and 51.3% of women have osteoporosis [6]. Concurrently, enhanced recovery pathways and patients' expectations for smaller incisions and early mobilization have accelerated the adoption of minimally invasive and endoscopic lumbar fusion (eg,

biportal endoscopic fusion) in recent years [7]. In elderly osteoporotic patients, low bone mass is a central clinical constraint, yet there is also a compelling need for less invasive treatment. Therefore, achieving clinically adequate posterior fixation stability under conditions of limited posterior exposure, as encountered in minimally invasive or endoscopic-assisted procedures, remains a particularly challenging clinical problem.

The fixation strength of traditional-trajectory pedicle screws (TT) largely relies on the mechanical properties of the pedicle and cancellous bone within the vertebral body, and screw loosening is more likely in osteoporotic bone [3]. To enhance screw purchase while meeting the requirements of limited posterior exposure, Santoni et al. proposed the cortical bone trajectory (CBT) technique [8], which increases pullout resistance through a more medial entry point and a higher proportion of cortical bone engagement and can be placed with less exposure. Clinical studies have suggested that, compared with conventional TT screws, CBT-based fixation may be associated with shorter operative time and less blood loss, while achieving comparable fusion rates and sagittal alignment maintenance [9–11]. However, the CBT trajectory and the manner in which loads are transferred at the screw–rod junction may predispose to more pronounced stress concentration and fatigue risk; furthermore, increased posterior-column constraint may alter global load transmission and affect the biomechanical environment of adjacent segments [12,13]. Accordingly, in osteoporotic TLIF settings where posterior exposure is limited, a fixation strategy is still needed that preserves the anatomic advantages of CBT while reducing high-stress exposure of key metallic components.

To address this need, we proposed a reverse cortical bone trajectory (reverse CBT, RCBT) screw strategy for reduced-exposure lumbar fusion. While maintaining a medial

entry point, the sagittal angulation of the caudal vertebral screw is reversed (caudally directed), with the intent of adjusting the force line and moment arm of the fixation unit, optimizing load transfer within the screw–rod system, dispersing stress, and improving the mechanical safety margin in osteoporosis. Systematic, multi-parameter comparisons among TT–TT, CBT–CBT, and CBT–RCBT constructs under both normal and osteoporotic conditions remain limited. Finite element analysis can quantify segmental stability, implant loading, and exposure-related geometric metrics under controlled loading conditions, providing an effective framework for such comparisons [14]. Therefore, a high-fidelity L3–S1 FE model was established and an L4–L5 TLIF scenario was simulated. Under both normal and osteoporotic conditions, the biomechanical performance of TT–TT, CBT–CBT, and CBT–RCBT fixation was compared to determine whether the CBT–RCBT construct could achieve a more favorable balance among construct stability, implant stress distribution, and reduced posterior exposure demand in TLIF.

Methods

2.1 Development of the intact lumbar finite element model

A three-dimensional lumbosacral FE model spanning L3–S1 was established (Fig. 1). Thin-slice computed tomography images (slice thickness ≤1.0 mm) were acquired from a healthy adult male without spinal pathology, and three-dimensional geometry was reconstructed. DICOM data were imported into Mimics (Materialise, Leuven, Belgium) for segmentation and initial reconstruction. The geometry was then imported into Geomagic Studio 12 (Geomagic, USA) for mesh repair and surface optimization, including re-triangulation, smoothing, triangle-size normalization, and NURBS surface

fitting to improve geometric fidelity. The optimized model was transferred to SolidWorks 2016 (Dassault Systèmes, USA) for detailed reconstruction and assembly of anatomic components, including vertebrae, the intervertebral disc (annulus fibrosus and nucleus pulposus), and facet joint cartilage. The assembled geometry was imported into HyperMesh 14.0 (Altair Engineering, USA) for FE meshing, and ligament structures as well as inter-tissue interactions were defined in Abaqus 6.14 (Dassault Systèmes, France). Mesh convergence analysis was performed using the intact L3 – S1 finite element model. Based on the method described by Ayturk et al. [15], axial rotation was selected for mesh convergence testing because it has been reported to be the loading mode most sensitive to mesh resolution in lumbar finite element models. Three mesh densities, denoted as Mesh 1, Mesh 2, and Mesh 3, were generated by progressively refining the global element size while maintaining the same geometry, material properties, boundary conditions, and loading protocol. Mesh 3 was used as the reference fine mesh. The percentage differences in von Mises stress of the major spinal components and L4 – L5 range of motion were calculated. Mesh convergence was considered achieved when the differences between Mesh 2 and Mesh 3 were less than 5% for all evaluated indicators. Based on this criterion, Mesh 2 was adopted for subsequent formal analyses. Model validation was performed at the L4–L5 segment by comparing the predicted ROM under flexion, extension, lateral bending, and axial rotation with previously reported in vitro and finite element data [16–18] (Fig. 2). The predicted L4–L5 ROMs fell within the ranges reported in the literature, supporting the use of the present model for subsequent comparative analyses.

2.2 Construction of TLIF models

Based on the intact model, a TLIF model was created at L4–L5. To simulate the extent of decompression and disc preparation in clinical TLIF, the facet cartilage, facet joints, annulus fibrosus, and nucleus pulposus at L4/5 were removed, and a portion of the cartilaginous endplate was excised to create working space. An interbody cage was inserted obliquely into the prepared disc space. With the cage position and decompression range held constant, three posterior fixation constructs were modeled: (1) bilateral traditional-trajectory pedicle screws (TT–TT); (2) bilateral cortical bone trajectory screws (CBT–CBT); and (3) a hybrid construct using cranially directed CBT at the cephalad vertebra and caudally directed reverse CBT at the caudal vertebra (CBT–RCBT). All models used identical posterior rods (diameter, 4.5 mm) and cages (length, 20 mm; height, 10–11 mm, adjusted slightly to match disc height). TT screws were 45 mm in length and 6.0 mm in diameter; CBT and RCBT screws were 35 mm in length and 5.0 mm in diameter. The CBT entry point was located at the junction of the inferior border of the transverse process and the midline of the superior articular process, with a cephalad angulation of 30°–45° and a lateral angulation of approximately 20°. The RCBT entry point was located in the superomedial quadrant of the pedicle projection (approximately the 11 o'clock position on the right, mirrored on the left), with a caudal angulation of 25°–30° and a lateral angulation of approximately 10° (Fig. 3, 4).

2.3 Material properties and interactions

Material properties for each tissue were assigned according to the literature [19–23] (Table 1). Cortical bone, cancellous bone, posterior elements, endplates, nucleus pulposus, annulus fibrosus, and ligaments were modeled as isotropic linear elastic materials. In contrast, the articular cartilage was defined as a Neo-Hookean hyperelastic

161 material. Hybrid tetrahedral elements were used for the cartilage component to account
162 for its near-incompressible behavior. Each vertebra consisted of a cortical shell,
163 cancellous bone, and superior/inferior endplates, with cortical thickness set to 1 mm.
164 Facet joints were modeled using surface-to-surface contact with a 0.5-mm joint gap and a
165 friction coefficient of 0.3; facet cartilage was represented as an independent structure
166 participating in contact. The cage–endplate, screw–rod, and screw–bone interfaces were
167 simplified using tie constraints to approximate a rigidly stabilized post-fusion construct
168 and to enable relative comparisons among fixation strategies under identical interface
169 assumptions[17]. The Young's modulus of the screws and rods was set to 110,000 MPa,
170 and the Young's modulus of the polyetheretherketone (PEEK) cage was set to 3,600 MPa.
171 An osteoporotic model was generated according to previously published lumbar finite
172 element studies [23, 24]. Relative to the normal-bone model, the Young's modulus of
173 cancellous bone was reduced by 66%, and the Young's modulus of cortical bone,
174 endplates, and posterior bony structures (including pedicles, laminae, and facet joints)
175 was reduced by 33%, whereas the remaining parameters were unchanged.

176 *2.4 Boundary and loading conditions*

177 Identical boundary and loading conditions were applied across all surgical models.
178 All degrees of freedom at the inferior surface of S1 were fully constrained. A 500-N
179 compressive follower load was applied along the curvature of the lumbar spine to
180 represent physiologic axial compression, followed by a superimposed 10 N·m moment to
181 simulate flexion, extension, lateral bending, and axial rotation [20]. This loading protocol
182 was adopted to facilitate comparative biomechanical analysis under standardized
183 conditions while better approximating physiologic load transfer than a simple axial

preload. Outcome measures included L4–L5 ROM, cage stress, peak stress in the posterior screw–rod system, and mean stress in adjacent-level discs (L3/4 and L5/S1), to compare the relative mechanical performance of the three fixation constructs under normal and osteoporotic conditions.

2.5 Quantification of posterior exposure demand

Posterior exposure demand was quantified using a geometric surrogate derived from standardized posterior-view projections of each three-dimensional construct. All constructs were evaluated under the same viewing orientation and scale. For each fixation strategy, a minimal boundary was delineated in ImageJ (National Institutes of Health, Bethesda, MD, USA) to encompass the posterior region required for screw insertion and rod connection. The measured area was defined as a pixel-based projected geometric area. The resulting normalized exposure area was interpreted as a geometric surrogate of posterior exposure demand rather than a direct indicator of actual soft-tissue injury or surgical invasiveness.

Results

3.1 Mesh convergence analysis

The mesh convergence analysis showed that the percentage differences between Mesh 2 and Mesh 3 were less than 5% for all evaluated spinal components and L4–L5 range of motion. Therefore, Mesh 2 was considered sufficiently converged and was used for all subsequent simulations. The detailed convergence results are shown in Fig. 5.

3.2 Segmental range of motion (ROM)

Detailed segmental ROM results under each loading mode are presented in Fig. 6 and Table 2. Under normal bone conditions, L4–L5 ROM in flexion was lowest in the

TT–TT construct (0.3058°) and highest in the CBT–RCBT construct (0.3890°). In extension, lateral bending, and axial rotation, the CBT–RCBT construct showed the lowest ROM (0.2777°, 0.5695°, and 0.2565°, respectively). Compared with CBT–CBT, the CBT–RCBT construct decreased ROM in extension, lateral bending, and rotation, but increased ROM in flexion. Compared with CBT–CBT, TT–TT showed lower ROM under all four loading modes, with reductions ranging from 4.20% to 14.32%. Under osteoporotic conditions, the CBT–CBT construct had the smallest flexion ROM (0.7159°). The CBT–RCBT construct exhibited the smallest ROM in extension, lateral bending, and axial rotation (0.4195°, 0.8978°, and 0.4268°, respectively), but the largest ROM in flexion (0.8604°). Compared with TT–TT, both CBT–CBT and CBT–RCBT reduced ROM under extension and rotational loading. In contrast, under flexion the CBT–RCBT construct demonstrated greater ROM than the other two constructs.

3.3 Maximum von Mises stresses of cages

Maximum von Mises stress in the interbody cage under each loading mode is summarized in Fig. 7 and Table 3. Under normal bone conditions, compared with TT–TT, both CBT–RCBT and CBT–CBT showed varying increases in cage stress across the four loading modes. In flexion, CBT–RCBT produced the highest peak cage stress (29.0000 MPa). In extension, lateral bending, and axial rotation, CBT–RCBT cage stress was 5.4300 MPa, 15.4150 MPa, and 16.9150 MPa, respectively, and was lower than that of CBT–CBT (6.6300 MPa, 16.5100 MPa, and 19.3400 MPa, respectively). Under osteoporotic conditions, overall patterns were similar. Compared with CBT–CBT, CBT–RCBT reduced cage stress in extension (7.8800 vs 8.0800 MPa), lateral bending (27.3700 vs 29.7250 MPa), and axial rotation (21.8500 vs 24.9350 MPa). In rotation, CBT–RCBT

was the lowest among the three constructs (21.8500 MPa), whereas it remained the highest under flexion (37.2000 MPa). Across constructs, cage stress increased with decreasing bone density.

3.4 Maximum von Mises stresses of posterior fixations

Maximum von Mises stress of the posterior fixation system under each loading mode is summarized in Fig. 8 and Table 4. Under normal bone conditions, the CBT–CBT construct exhibited the highest peak von Mises stress under all loading modes (flexion, 115.5609 MPa; extension, 167.7205 MPa; lateral bending, 248.7601 MPa; axial rotation, 258.5911 MPa). In contrast, the TT–TT construct had the lowest peak stress in flexion, extension, and lateral bending (60.5312 MPa, 134.3387 MPa, and 161.5988 MPa, respectively). Under axial rotation, CBT–RCBT demonstrated the lowest peak stress (104.6902 MPa), lower than TT–TT (167.7808 MPa) and CBT–CBT (258.5911 MPa). Relative to CBT–CBT, CBT–RCBT reduced peak stress in all four directions by 10.93%–59.52%, with the largest reduction under axial rotation (59.52%). Regarding loading direction, peak stress occurred under axial rotation for TT–TT and CBT–CBT (167.7808 MPa and 258.5911 MPa, respectively), whereas for CBT–RCBT peak stress occurred under lateral bending (186.6200 MPa), and the lowest value occurred under flexion (84.2504 MPa). Under osteoporotic conditions, peak stress in all three constructs increased compared with the normal-bone condition. CBT–CBT remained the highest under all loading modes (flexion, 183.6010 MPa; extension, 211.0003 MPa; lateral bending, 334.6087 MPa; axial rotation, 302.1203 MPa). TT–TT was lowest under flexion and lateral bending (93.1789 MPa and 205.2408 MPa), whereas CBT–RCBT was lowest under extension and axial rotation (174.3510 MPa and 142.6792 MPa). Compared with

CBT–CBT, CBT–RCBT reduced peak stress in all directions by 17.37%–52.77%, again with the greatest reduction under axial rotation. Von Mises stress contour plots demonstrated that, in the osteoporotic model, high-stress regions (yellow–red) were primarily concentrated at the screw head–rod junction and at the screw neck/proximal threads across all fixation strategies (Fig. 9).

3.5 Mean von Mises stresses of intervertebral discs

Mean adjacent-level disc stress values and corresponding stress contours are presented in Figs. 10 and 11 and summarized in Tables 5 and 6. Under normal bone conditions, mean stress at the superior adjacent disc (L3/4) varied within a narrow range across constructs. During flexion, TT–TT showed the lowest value (0.2378 MPa), whereas CBT–RCBT showed the highest value (0.2500 MPa). During extension and lateral bending, CBT–RCBT showed the lowest values (0.3467 MPa and 0.3733 MPa, respectively), whereas CBT–CBT showed the highest values (0.3671 MPa and 0.3795 MPa, respectively). During axial rotation, L3/4 stress ranged from 0.3063 to 0.3067 MPa. At the inferior adjacent disc (L5/S1), mean stress also varied within a narrow range. During flexion, TT–TT showed the lowest value (0.2874 MPa), whereas CBT–RCBT showed the highest value (0.3163 MPa). During extension, CBT–CBT showed the lowest value (0.1591 MPa), whereas TT–TT showed the highest value (0.1843 MPa). During lateral bending and axial rotation, L5/S1 stress ranged from 0.2703 to 0.2808 MPa and from 0.2263 to 0.2347 MPa, respectively. Under osteoporotic conditions, a similar distribution pattern was observed. At L3/4, CBT–RCBT showed the lowest values during extension and lateral bending (0.3445 MPa and 0.3757 MPa, respectively), whereas during flexion it showed a higher value than CBT–CBT (0.2537 vs 0.2466 MPa). During

axial rotation, L3/4 stress ranged from 0.3075 to 0.3079 MPa across constructs. At L5/S1, CBT–RCBT showed a higher flexion stress than CBT–CBT (0.3309 vs 0.3187 MPa), whereas CBT–CBT showed the lowest extension stress (0.1571 MPa). During lateral bending and axial rotation, L5/S1 stress ranged from 0.2742 to 0.2833 MPa and from 0.2372 to 0.2486 MPa, respectively.

3.6 Posterior exposure requirement

To quantify posterior exposure requirements among screw-placement strategies, the posterior exposure area required for screw insertion and rod connection was measured from standardized posterior-view projections and normalized to the TT–TT construct (set as 1). The relative posterior exposure areas were 1, 0.6988, and 0.4038 for TT–TT, CBT–CBT, and CBT–RCBT, respectively (Fig. 12).

Discussion

Elderly patients with osteoporosis undergoing TLIF often face two competing challenges: the need to limit posterior exposure to reduce soft-tissue disruption, and the reduced screw purchase associated with low bone mass, which may increase the mechanical burden on posterior instrumentation [25,26]. Within this context, the present findings suggest that, under osteoporotic conditions, the CBT–RCBT construct (cephalad CBT combined with caudal reverse CBT) may offer a more favorable biomechanical profile than CBT–CBT, characterized by improved construct stability in extension, lateral bending, and axial rotation and lower stress in the screw–rod system. Meanwhile, posterior exposure demand was markedly lower than that of both TT–TT and CBT–CBT. Importantly, these potential advantages were not accompanied by a consistent increase in adjacent-level disc stress, although cage loading remained direction-dependent.

Residual ROM at the fused segment after TLIF is a key quantitative index of construct rigidity and stability and has been linked to complications such as pseudarthrosis and cage subsidence [27]. Under normal bone conditions, TT–TT generally demonstrated smaller ROM values and thus retained an overall stability advantage, whereas CBT–CBT showed higher ROM than TT–TT in most directions. Under osteoporotic conditions, CBT–CBT reduced ROM relative to TT–TT in certain directions but did not provide consistent improvement across all motions, indicating that CBT–CBT alone may not comprehensively enhance multidirectional stability. These findings are consistent with prior biomechanical investigations [28–30]. By contrast, CBT–RCBT provided smaller residual ROM under extension, lateral bending, and rotation, suggesting improved construct stability under extension, lateral bending, and axial rotation in the present model. Mechanistically, the caudally directed trajectory of the caudal screw in CBT–RCBT may optimize force transmission and enhance torsional resistance, which may contribute to a more favorable mechanical environment. Notably, stability gains in flexion were not the most prominent, indicating a degree of direction dependence. Clinically, optimization of anterior-column support and sagittal alignment management (eg, adequate disc-height restoration and endplate preservation) may further improve overall stability under flexion.

An increase in peak cage stress is generally interpreted as a higher risk of endplate subsidence over time [31]. Under normal bone conditions, TT–TT produced lower cage loading overall, suggesting an advantage in reducing cage–endplate interface stress. Under osteoporotic conditions, cage stress shifted upward across constructs, reflecting diminished endplate support and greater load sharing by the cage, which increases the

baseline risk of subsidence. Within this context, when CBT-based fixation is preferred for endoscopic/channel-based procedures, CBT–RCBT further reduced peak cage stress in multiple motion directions compared with standard CBT–CBT. This finding suggests that CBT–RCBT may offer a more favorable cage loading profile under selected loading conditions, with potential implications for maintaining anterior column support and disc space stability in osteoporotic TLIF. In clinical practice, endplate-preserving techniques and anterior-column support strategies (eg, selecting a cage with a larger footprint, avoiding excessive endplate preparation, and managing early postoperative loading) may consolidate this potential benefit.

Fatigue fracture of the screw–rod system is a major contributor to late mechanical failure, and risk is closely related to peak stress and stress concentration at junctional regions [32]. In the normal-bone model, TT–TT demonstrated lower peak stress in multiple directions, whereas CBT–CBT exhibited higher peak stress across all modes, suggesting a less favorable stress environment at the connection region. In the osteoporotic model, peak stress increased across constructs, indicating that low bone mass amplifies mechanical demands on instrumentation [33]. More clinically relevant, CBT–RCBT reduced peak stress relative to CBT–CBT in all loading directions under osteoporotic conditions. These results imply that CBT–RCBT may decrease high-stress exposure at critical junctions, thereby providing a more favorable stress environment for the posterior instrumentation.

Adjacent segment disease (ASD) is a multifactorial event associated with age, number of fused levels, fusion duration, construct stiffness, and pre-existing adjacent-level degeneration [34,35]. Prior studies have suggested that post-fusion stiffness alterations

may influence load distribution to adjacent segments and contribute to ASD development [36]. In this study, mean adjacent-level disc stress was used as a surrogate indicator of load transfer for relative comparisons among constructs. Across both normal and osteoporotic conditions, differences in mean disc stress at L3/4 and L5/S1 were numerically limited and did not show a consistent increase for any single construct. Under the present boundary conditions and loading protocol, these findings suggest that CBT–RCBT does not exhibit a more unfavorable adjacent-level load transfer pattern than TT–TT or CBT–CBT.

The extent of paraspinal muscle detachment is critical to realizing the potential benefits of minimally invasive/endoscopic fusion. Previous studies have shown that greater retraction and detachment in traditional posterior approaches may be associated with muscle ischemia, atrophy, and functional deterioration and may increase postoperative pain burden and degeneration risk [37,38]. In comparative studies of fusion techniques, minimally invasive strategies are typically associated with less paraspinal muscle injury and may facilitate more favorable early recovery [39]. Here, posterior exposure area was used as a surrogate for paraspinal muscle detachment demand, following the quantification approach used in prior TLIF FE work [39]. Using a posterior-view projection of the three-dimensional model, the minimal exposure boundary required for screw insertion and rod connection was delineated for each construct, and the corresponding area was calculated and normalized to TT–TT (set as 1). Compared with TT–TT, exposure requirements were reduced by approximately 30.12% for CBT–CBT and 59.62% for CBT–RCBT; compared with CBT–CBT, CBT–RCBT further reduced exposure by approximately 42.2%. These results are consistent with the anatomic

advantage of CBT screws—namely, a more medial entry point and reduced lateral exposure requirements [9,40]—and suggest potential relevance of CBT-based screw placement to reduced-exposure or channel-based approaches. Importantly, CBT–RCBT further narrowed the required exposure while preserving the medial entry-point advantage of CBT–CBT. A plausible mechanism is that the caudally directed trajectory at the caudal level alters the spatial relationship between the screw head and the rod, resulting in a more compact screw–rod configuration and reducing the necessary extent of retraction and detachment. Clinically, this may further decrease soft-tissue trauma in elderly osteoporotic patients and promote smoother early functional recovery and rehabilitation [40]. Taken together with the stability and instrumentation-stress findings under osteoporotic conditions, the exposure advantage of CBT–RCBT was not achieved at the expense of reduced mechanical safety margins. This geometric reduction in posterior exposure demand highlights a potential advantage of the CBT–RCBT construct and may be particularly meaningful in reduced-exposure fusion strategies for osteoporotic TLIF, such as minimally invasive or endoscopic-assisted approaches.

Given its favorable biomechanical performance and lower posterior exposure demand in the present model, the CBT–RCBT construct may represent a promising concept for reduced-exposure fusion strategies. Its potential relevance in minimally invasive or endoscopic-related TLIF settings warrants further biomechanical and clinical investigation, as these operative scenarios were not directly simulated in the current study.

Several limitations inherent to FE modeling should be acknowledged. Active contraction and dynamic stabilization by the lumbar musculature were not explicitly

modeled; only passive stabilizing structures were represented via ligaments and contact relationships, which may affect the physiologic reproduction of load transfer and dynamic stability and lead to deviations in absolute ROM and stress values from in vivo conditions. Quasi-static loading was applied, and long-term cyclic behavior could not be predicted, including the evolution of rod fatigue, screw loosening, and the influence of bone remodeling on interface mechanics. In addition, posterior exposure was quantified using a geometric surrogate rather than a direct clinical measure of soft-tissue injury, and this should be considered when interpreting the exposure-related findings. Nevertheless, under unified geometry, boundary conditions, material definitions, and implant parameters, this study provides a valuable basis for comparing the relative mechanical performance of TT–TT, CBT–CBT, and CBT–RCBT constructs under normal and osteoporotic conditions and provides a biomechanical basis for future evaluation of CBT–RCBT in reduced-exposure fusion strategies.

Conclusions

Under osteoporotic conditions, hybrid CBT–RCBT fixation improved construct stability in extension, lateral bending, and axial rotation and reduced posterior screw–rod stress relative to CBT–CBT, while it also substantially decreased posterior exposure requirements. These findings support further biomechanical and clinical evaluation of CBT–RCBT instrumentation in osteoporotic TLIF, particularly in surgical scenarios where reduced posterior exposure is desirable.

Declarations

Ethics approval and consent to participate

The study was approved by the Medical Ethics Committee of Qilu Hospital of Shandong University (Approval No. KLYY-2026-02-068-1) on May 12, 2026. All procedures involving human data were performed in accordance with the Declaration of Helsinki and relevant guidelines and regulations. Written informed consent was obtained from the volunteer whose computed tomography data were used for model reconstruction.

Consent for publication

Not applicable.

Availability of data and materials

The datasets used and/or analysed during the current study are available from the corresponding author on reasonable request.

Competing interests

The authors declare that they have no competing interests.

Funding

This work was supported by the Shandong Provincial Natural Science Foundation (No. ZR2023MH285), the Shandong Provincial Key Research and Development Program (Innovation Capacity Enhancement Project for Technology-based Small and Medium-sized Enterprises; No. 2025TSGCCZZB0448), the Shandong Provincial Medical Association (No. YXH2025YS101), and the 2025 Research and Evaluation Project of the China Association of Chinese Medicine (Special Project on Traditional Chinese Medicine; No. CACMREZZ2025-A-22).

Clinical trial number:

Not applicable.

Authors' contributions

W.X. and H.S. conceived and designed the study. X.W. curated the data. X.Z. and W.Z. performed the investigation. Y.F. and X.L. conducted the formal analysis. C.L., X.L. and Z.K. developed the methodology. K.W. and X.G. performed the software implementation. K.W., Z.K. and H.S. carried out the validation. X.L., Z.K. and H.S. drafted the original manuscript. W.X., Z.K. and H.S. reviewed and edited the manuscript. All authors read and approved the final manuscript.

Acknowledgements

The authors thank the Department of Orthopedics, Qilu Hospital of Shandong University, for institutional support.

List of abbreviations:

TLIF: Transforaminal lumbar interbody fusion

TT: Traditional trajectory

CBT: Cortical bone trajectory

RCBT: Reverse cortical bone trajectory

TT-TT: Bilateral traditional-trajectory pedicle screw fixation

CBT-CBT: Bilateral cortical bone trajectory screw fixation

CBT-RCBT: Hybrid fixation using cranially directed CBT and caudally directed reverse CBT

FE: Finite element

ROM: Range of motion

PEEK: Polyetheretherketone

ASD: Adjacent segment disease

References

1. Farber SH, Dugan RK, White MD, et al. A comparison of modern-era anterior lumbar interbody fusion and minimally invasive transforaminal lumbar interbody fusion at the lumbosacral junction. J Neurosurg Spine. 2023;39(6):785–792.
2. Lidar Z, Beaumont A, Lifshutz J, et al. Clinical and radiological relationship between posterior lumbar interbody fusion and posterolateral lumbar fusion. Surg Neurol. 2005;64:303–8.
3. Zhong C, Han Z. Biomechanical optimization of pedicle screw trajectories in osteoporotic lumbar fusion: finite element analysis and validation of robotic-assisted implementation. J Robot Surg. 2025;20(1):99.
4. Mi J, Li K, Zhao X, et al. Vertebral body Hounsfield units are associated with cage subsidence after transforaminal lumbar interbody fusion with unilateral pedicle screw fixation. Clin Spine Surg. 2017;30(8):E1130–E1136.
5. Meredith DS, Schreiber JJ, Taher F, et al. Lower preoperative Hounsfield unit measurements are associated with adjacent segment fracture after spinal fusion. Spine (Phila Pa 1976). 2013;38(5):415–8.
6. Chin DK, Park JY, Yoon YS, et al. Prevalence of osteoporosis in patients requiring spine surgery: incidence and significance of osteoporosis in spine disease. Osteoporos Int. 2007;18:1219–24.
7. Heo DH, Park CK. Clinical results of percutaneous biportal endoscopic lumbar interbody fusion with application of enhanced recovery after surgery. Neurosurg Focus. 2019;46(4):E18.

8. Santoni BG, Hynes RA, McGilvray KC, et al. Cortical bone trajectory for lumbar pedicle screws. Spine J. 2009;9(5):366–373.
9. Lee GW, Son JH, Ahn MW. The comparison of pedicle screw and cortical screw in posterior lumbar interbody fusion: a prospective randomized noninferiority trial. Spine J. 2015;15(7):1519–1526.
10. Zheng J, Wu Y, Guo C, et al. Efficacy and safety of cortical bone trajectory screws versus pedicle screws in lumbar fusion: a systematic review and meta-analysis. World Neurosurg. 2024;188:e233–e246.
11. Kasukawa Y, Miyakoshi N, Hongo M, et al. Short-term results of transforaminal lumbar interbody fusion using pedicle screw with cortical bone trajectory compared with conventional trajectory. Asian Spine J. 2015;9(3):440–448.
12. Calvert GC, Lawrence BD, Abtahi AM, et al. Cortical screws used to rescue failed lumbar pedicle screw constructs: a biomechanical analysis. J Neurosurg Spine. 2015;22(2):166–172.
13. Wang Y, Liu H, Li B, et al. Three different screw trajectories in single segment fixation: a finite element analysis and biomechanical study. Spine J. 2025;25(7):1552–1563.
14. Viceconti M, Clapworthy G, Van Sint Jan S, et al. The virtual physiological human - a European initiative for in silico human modelling. J Physiol Sci. 2008;58:441–6.
15. Ayturk UM, Puttlitz CM. Parametric convergence sensitivity and validation of a finite element model of the human lumbar spine. Comput Methods Biomech Biomed Engin. 2011;14(8):695-705.

16. Shim CS, Park SW, Lee SH, et al. Biomechanical evaluation of an interspinous stabilizing device, Locker. Spine (Phila Pa 1976). 2008;33(22):E820–E827.
17. Sin DA, Heo DH. Comparative finite element analysis of lumbar cortical screws and pedicle screws in transforaminal and posterior lumbar interbody fusion. Neurospine. 2019;16(2):298–304.
18. Zhong ZC, Hung C, Lin HM, et al. The influence of different magnitudes and methods of applying preload on fusion and disc replacement constructs in the lumbar spine: a finite element analysis. Comput Methods Biomech Biomed Engin. 2013;16(9):943–953.
19. Fan W, Guo LX. Finite element investigation of the effect of nucleus removal on vibration characteristics of the lumbar spine under a compressive follower preload. J Mech Behav Biomed Mater. 2018;78:342–51.
20. He L, Xiang Q, Yang Y, et al. The anterior and traverse cage can provide optimal biomechanical performance for both traditional and percutaneous endoscopic transforaminal lumbar interbody fusion. Comput Biol Med. 2021;131:104291.
21. Wang QD, Guo LX. Biomechanical role of cement augmentation in the vibration characteristics of the osteoporotic lumbar spine after lumbar interbody fusion. J Mater Sci Mater Med. 2022;33:52.
22. Shen H, Zhu J, Huang C, et al. Effect of interbody implants on the biomechanical behavior of lateral lumbar interbody fusion: a finite element study. J Funct Biomater. 2023;14:113.
23. Zhang G, Li J, Zhang L, et al. Biomechanical effect of different posterior fixation techniques on stability and adjacent segment degeneration in treating thoracolumbar

burst fracture with osteoporosis: a finite element analysis. Spine (Phila Pa 1976). 2024;49(15):E229–E238.

24. Polikeit A, Nolte LP, Ferguson SJ. The effect of cement augmentation on the load transfer in an osteoporotic functional spinal unit: finite-element analysis. Spine (Phila Pa 1976). 2003;28:991–6.

25. Ebata S, Takahashi J, Hasegawa T, et al. Role of weekly teriparatide administration in osseous union enhancement within six months after posterior or transforaminal lumbar interbody fusion for osteoporosis-associated lumbar degenerative disorders: a multicenter, prospective randomized study. J Bone Joint Surg Am. 2017;99:365–72.

26. Khalid SI, Nunna RS, Maasarani S, et al. Association of osteopenia and osteoporosis with higher rates of pseudarthrosis and revision surgery in adult patients undergoing single-level lumbar fusion. Neurosurg Focus. 2020;49(2):E6.

27. Burkhard MD, Spirig JM, Wanivenhaus F, et al. Residual motion of different posterior instrumentation and interbody fusion constructs. Eur Spine J. 2023;32(4):1411–1420.

28. Liu C, Zhao M, Zhang W, et al. Biomechanical assessment of different transforaminal lumbar interbody fusion constructs in normal and osteoporotic condition: a finite element analysis. Spine J. 2024;24(6):1121–1131.

29. Matsukawa K, Yato Y, Imabayashi H, et al. Biomechanical evaluation of the fixation strength of lumbar pedicle screws using cortical bone trajectory: a finite element study. J Neurosurg Spine. 2015;23:471–8.

30. Matsukawa K, Yato Y, Imabayashi H, et al. Biomechanical evaluation of lumbar pedicle screws in spondylolytic vertebrae: comparison of fixation strength between

the traditional trajectory and a cortical bone trajectory. J Neurosurg Spine. 2016;24:910–5.

31. Kim M-C, Chung HT, Cho JL, et al. Subsidence of polyetheretherketone cage after minimally invasive transforaminal lumbar interbody fusion. J Spinal Disord Tech. 2013;26:87–92.
32. Fan W, Guo LX, Zhao D. Stress analysis of the implants in transforaminal lumbar interbody fusion under static and vibration loadings: a comparison between pedicle screw fixation system with rigid and flexible rods. J Mater Sci Mater Med. 2019;30(10):118.
33. Liu ZX, Gao ZW, Chen C, et al. Effects of osteoporosis on the biomechanics of various supplemental fixations co-applied with oblique lumbar interbody fusion (OLIF): a finite element analysis. BMC Musculoskelet Disord. 2022;23(1):794.
34. Sakaura H, Ikegami D, Fujimori T, et al. Early cephalad adjacent segment degeneration after posterior lumbar interbody fusion: a comparative study between cortical bone trajectory screw fixation and traditional trajectory screw fixation. J Neurosurg Spine. 2019;32:155–9.
35. Cheh G, Bridwell KH, Lenke LG, et al. Adjacent segment disease following lumbar/thoracolumbar fusion with pedicle screw instrumentation: a minimum 5-year follow-up. Spine (Phila Pa 1976). 2007;32:2253–7.
36. Yan J-Z, Qiu GX, Wu ZH, et al. Finite element analysis in adjacent segment degeneration after lumbar fusion. Int J Med Robot. 2011;7:96–100.
37. Gille O, Jolivet E, Dousset V, et al. Muscle changes after posterior lumbar surgery: a quantitative MRI study. Spine (Phila Pa 1976). 2007;32(11):1230–1235.

38. Stevens KJ, Spenciner DB, Griffiths KL, et al. Comparison of minimally invasive and conventional open posterolateral lumbar fusion using magnetic resonance imaging and clinical outcomes. Spine (Phila Pa 1976). 2006;31(6):720–727.
39. Tuoheti Y, Li X, Zhang Z, et al. Biomechanical evaluation of modified and traditional cortical bone trajectory technique on adjacent segment degeneration in transforaminal lumbar interbody fusion: a finite element analysis. BMC Musculoskelet Disord. 2024;25:7.
40. Mobbs RJ, Sivabalan P, Li J. Technique, challenges and indications for cortical bone trajectory screws in lumbar spine surgery. J Clin Neurosci. 2016;26:16–22.

Table 1 Material properties of the finite element model

Component	Young's modulus (MPa)	Poisson ratio	Cross-sectional area (mm^2)
Vertebral body			
Cortical bone	12000 (osteoporosis: 8040)	0.3	—
Cancellous bone	100 (osteoporosis: 34)	0.2	—
Endplate	1000 (osteoporosis: 670)	0.3	—
Posterior bone	3500 (osteoporosis: 2345)	0.3	—
Screws and rods	110000	0.29	—
PEEK cage	3600	0.49	—
Nucleus pulposus	1	0.45	—
Annulus fibrosus	4.2	0.3	—
Articular cartilage	Neo-Hookean, C10 = 30, D1 = 0	—	—
Ligaments			
Anterior longitudinal ligament	20	0.3	63.7
Posterior longitudinal ligament	20	0.3	20
Interspinous ligament	11.6	0.3	40
Supraspinous ligament	15	0.3	30
Intertransverse ligament	58.7	0.3	3.6
Capsular ligament	32.9	0.3	60
Ligamentum flavum	19.5	0.3	40

Values for the osteoporotic model are shown in parentheses.

Abbreviation: PEEK, polyetheretherketone.

Table 2. Segmental range of motion of the L4–L5 fusion segment under normal and osteoporotic conditions

Segmental range of motion (ROM) of the L4–L5 fusion segment (°)						
Loading mode	Normal			Osteoporosis		
	TT–TT	CBT–CBT	CBT–RCBT	TT–TT	CBT–CBT	CBT–RCBT
Flexion	0.3058	0.3192	0.3890	0.7662	0.7159	0.8604
Extension	0.3205	0.3425	0.2777	0.6264	0.4417	0.4195
Lateral bending	0.6095	0.7114	0.5695	0.9474	1.1149	0.8978
Rotation	0.3973	0.4216	0.2565	0.7205	0.5517	0.4268

Abbreviation: TT–TT, bilateral traditional-trajectory pedicle screw fixation; CBT–CBT, bilateral cortical bone trajectory screw fixation; CBT–RCBT, hybrid fixation using cranially directed CBT and caudally directed reverse CBT.

Table 3. Maximum von Mises stress of the interbody cage under normal and osteoporotic conditions

Maximum von Mises stress of the interbody cage (MPa)						
Loading mode	Normal			Osteoporosis		
	TT–TT	CBT–CBT	CBT–RCBT	TT–TT	CBT–CBT	CBT–RCBT
Flexion	24.8300	26.7900	29.0000	34.7700	36.4000	37.2000
Extension	5.3200	6.6300	5.4300	7.1000	8.0800	7.8800
Lateral bending	14.7050	16.5100	15.4150	25.1600	29.7250	27.3700
Rotation	16.7800	19.3400	16.9150	23.9250	24.9350	21.8500

Abbreviation: TT–TT, bilateral traditional-trajectory pedicle screw fixation; CBT–CBT, bilateral cortical bone trajectory screw fixation; CBT–RCBT, hybrid fixation using cranially directed CBT and caudally directed reverse CBT.

Table 4. Maximum von Mises stress of the posterior screw–rod system under normal and osteoporotic conditions

Maximum von Mises stress of the posterior screw–rod system (MPa)						
Loading mode	Normal			Osteoporosis		
	TT–TT	CBT–CBT	CBT–RCBT	TT–TT	CBT–CBT	CBT–RCBT
Flexion	60.5312	115.5609	84.2504	93.1789	183.6010	122.0894
Extension	134.3387	167.7205	149.3899	190.8111	211.0003	174.3510
Lateral bending	161.5988	248.7601	186.6200	205.2408	334.6087	252.5807
Rotation	167.7808	258.5911	104.6902	206.5297	302.1203	142.6792

Abbreviation: TT–TT, bilateral traditional-trajectory pedicle screw fixation; CBT–CBT, bilateral cortical bone trajectory screw fixation; CBT–RCBT, hybrid fixation using cranially directed CBT and caudally directed reverse CBT.

Table 5. Mean von Mises stress of the superior adjacent intervertebral disc (L3/4) under normal and osteoporotic conditions

Mean von Mises stress of the L3/4 intervertebral disc (MPa)						
Loading mode	Normal			Osteoporosis		
	TT–TT	CBT–CBT	CBT–RCBT	TT–TT	CBT–CBT	CBT–RCBT
Flexion	0.2378	0.2434	0.2500	0.2414	0.2466	0.2537
Extension	0.3593	0.3671	0.3467	0.3561	0.3636	0.3445
Lateral bending	0.3783	0.3795	0.3733	0.3798	0.3820	0.3757
Rotation	0.3063	0.3066	0.3067	0.3079	0.3075	0.3079

Abbreviation: TT–TT, bilateral traditional-trajectory pedicle screw fixation; CBT–CBT, bilateral cortical bone trajectory screw fixation; CBT–RCBT, hybrid fixation using cranially directed CBT and caudally directed reverse CBT.

Table 6. Mean von Mises stress of the inferior adjacent intervertebral disc (L5/S1) under normal and osteoporotic conditions

Mean von Mises stress of the L5/S1 intervertebral disc (MPa)						
Loading mode	Normal			Osteoporosis		
	TT–TT	CBT–CBT	CBT–RCBT	TT–TT	CBT–CBT	CBT–RCBT
Flexion	0.2874	0.3044	0.3163	0.2996	0.3187	0.3309
Extension	0.1843	0.1591	0.1772	0.1888	0.1571	0.1805
Lateral bending	0.2808	0.2703	0.2715	0.2833	0.2742	0.2758
Rotation	0.2347	0.2263	0.2299	0.2486	0.2372	0.2427

Abbreviation: TT–TT, bilateral traditional-trajectory pedicle screw fixation; CBT–CBT, bilateral cortical bone trajectory screw fixation; CBT–RCBT, hybrid fixation using cranially directed CBT and caudally directed reverse CBT.

Figure 1. Frontal and lateral views of the intact lumbosacral finite element model.

Legend: (A) Frontal view. (B) Lateral view. The model represents the reconstructed healthy adult lumbosacral spine used for subsequent finite element analysis.

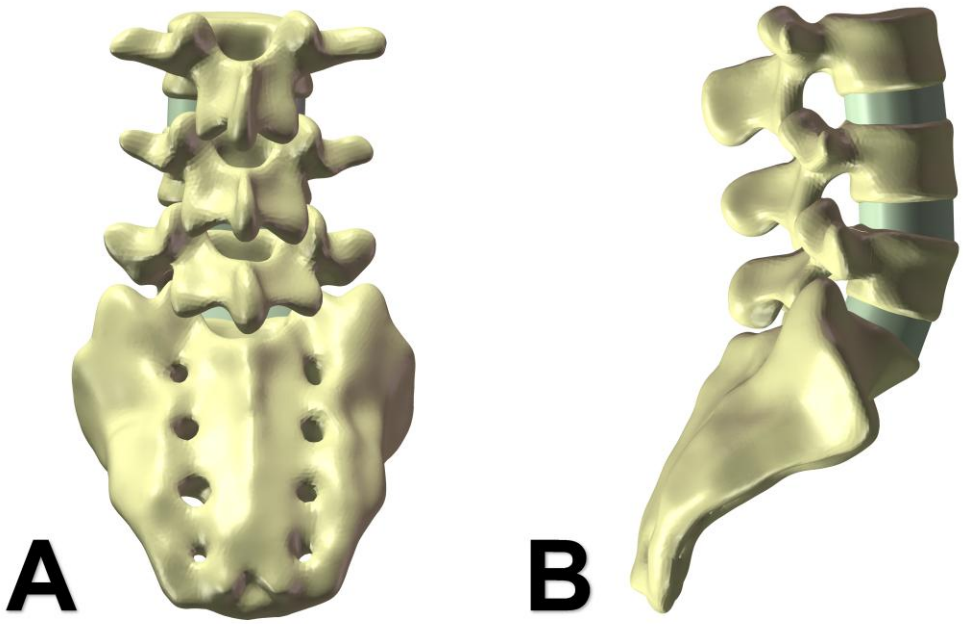


Figure 2. Validation of the intact L4–L5 finite element model.

Legend: The predicted L4–L5 range of motion (ROM) under flexion, extension, lateral bending, and axial rotation was compared with previously published in vitro and finite element data. The predicted values were generally within the reported ranges.

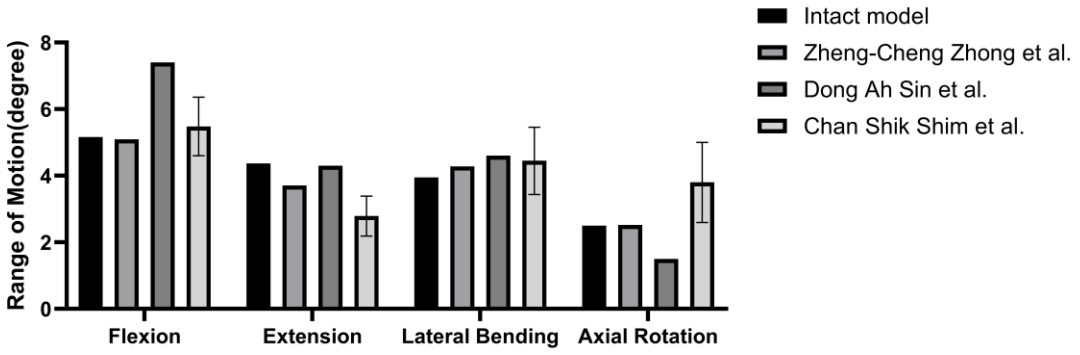


Figure 3. Frontal view of the three TLIF fixation constructs.

Legend: (A) Bilateral traditional-trajectory pedicle screw fixation (TT–TT). (B) Bilateral cortical bone trajectory screw fixation (CBT–CBT). (C) Hybrid fixation using cranially directed CBT and caudally directed reverse CBT (CBT–RCBT).

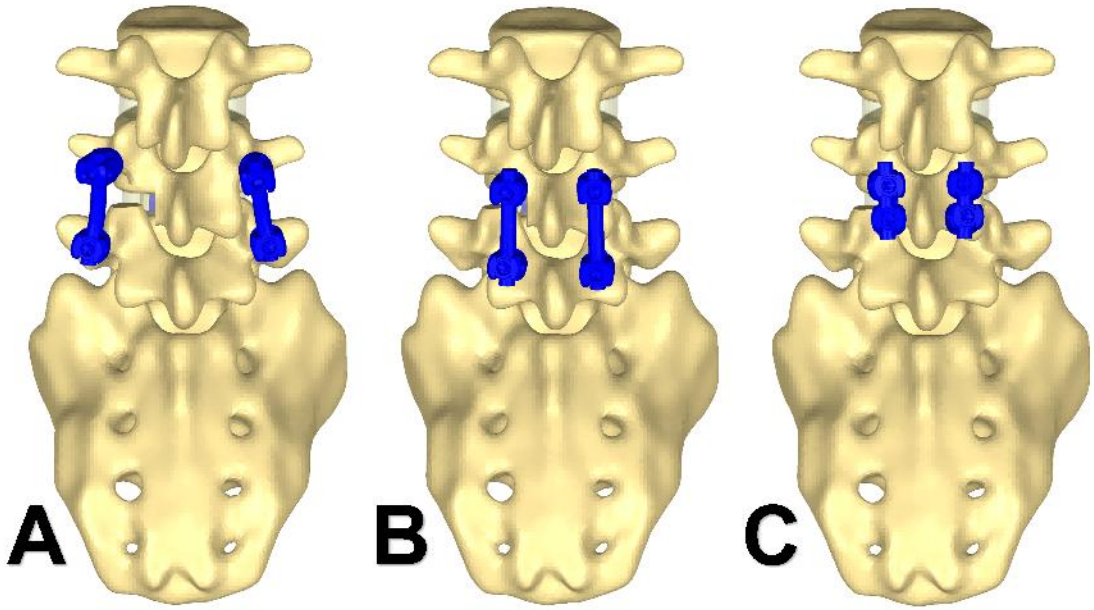


Figure 4. Lateral view of the three TLIF fixation constructs.

Legend: (A) Bilateral traditional-trajectory pedicle screw fixation (TT–TT). (B) Bilateral cortical bone trajectory screw fixation (CBT–CBT). (C) Hybrid fixation using cranially directed CBT and caudally directed reverse CBT (CBT–RCBT).

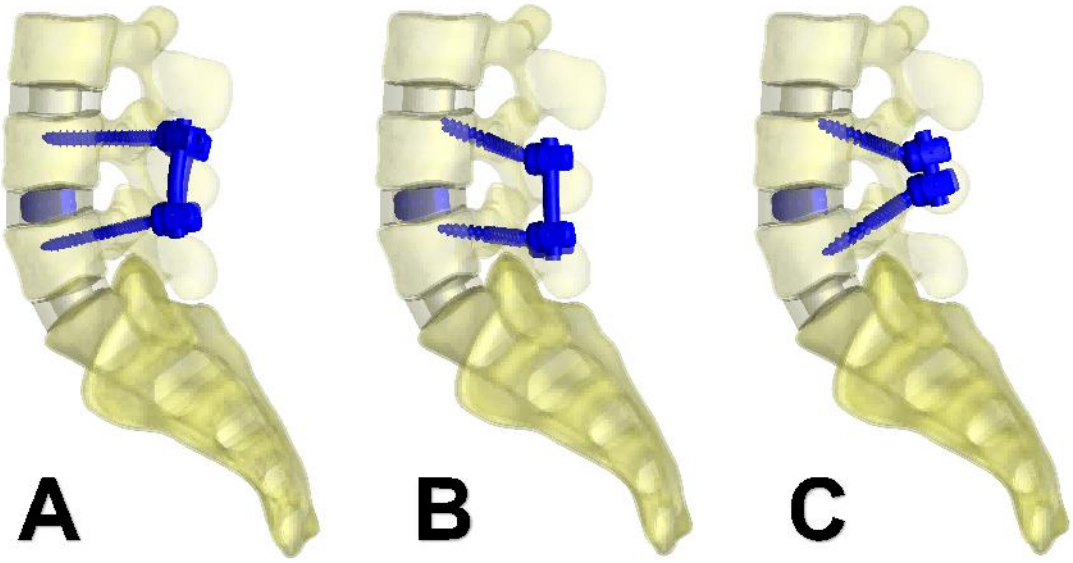


Figure 5. Mesh convergence analysis of the intact L3–S1 finite element model.

Legend: Mesh 3 was used as the reference fine mesh. The percentage differences between Mesh 2 and Mesh 3 were less than 5% for all evaluated spinal components and L4–L5 range of motion, indicating that Mesh 2 provided adequate numerical stability for subsequent finite element analyses.

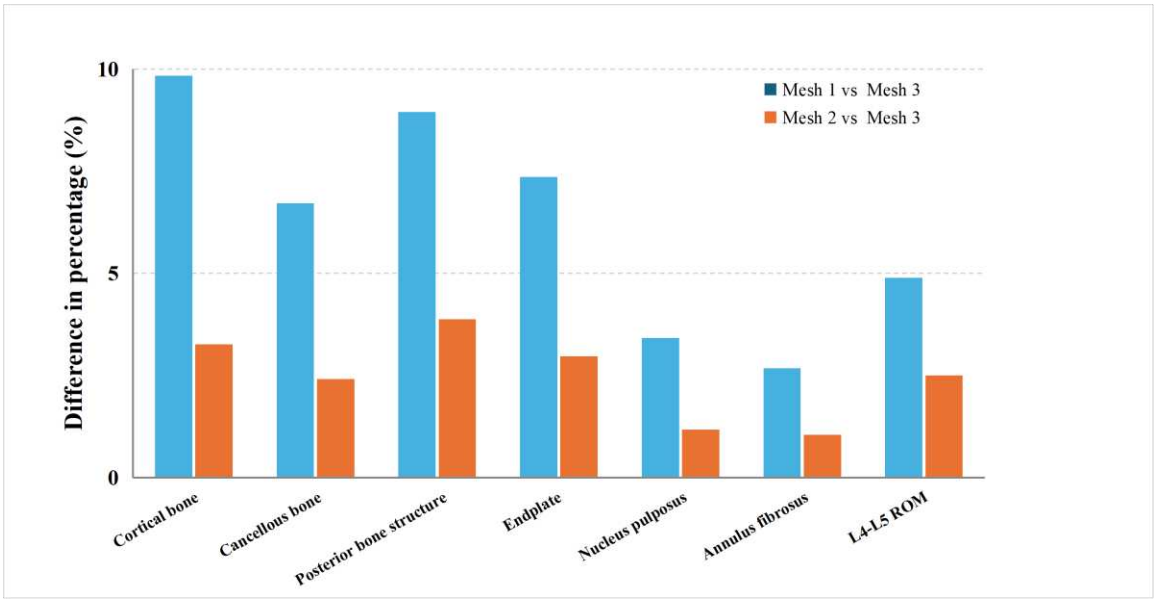


Figure 6. L4–L5 ROM under normal and osteoporotic conditions.

Legend: Segmental range of motion (ROM) of the L4–L5 fusion segment in the TT–TT, CBT–CBT, and CBT–RCBT models under normal and osteoporotic conditions. For consistency with the terminology used in the main text, the figure labels TTS, CBTS, and RCBT correspond to TT-TT, CBT-CBT, and CBT-RCBT, respectively.

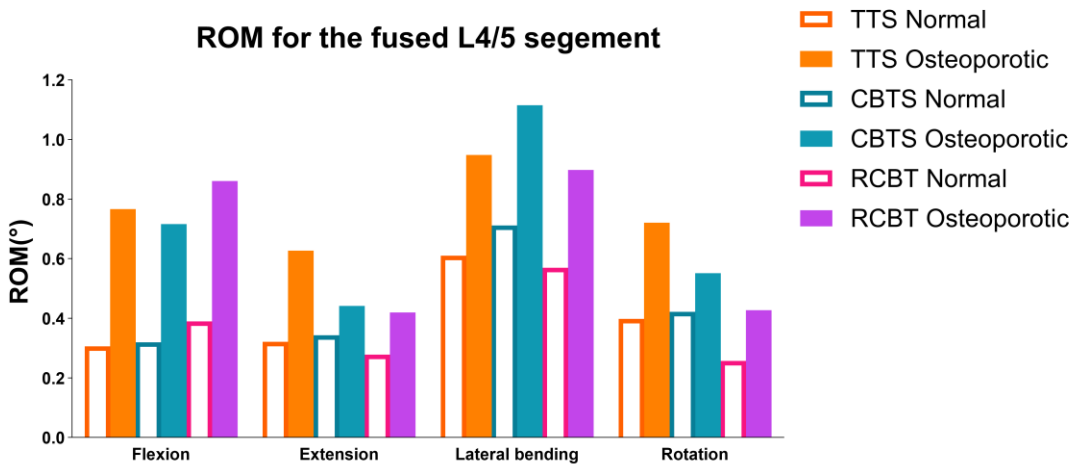
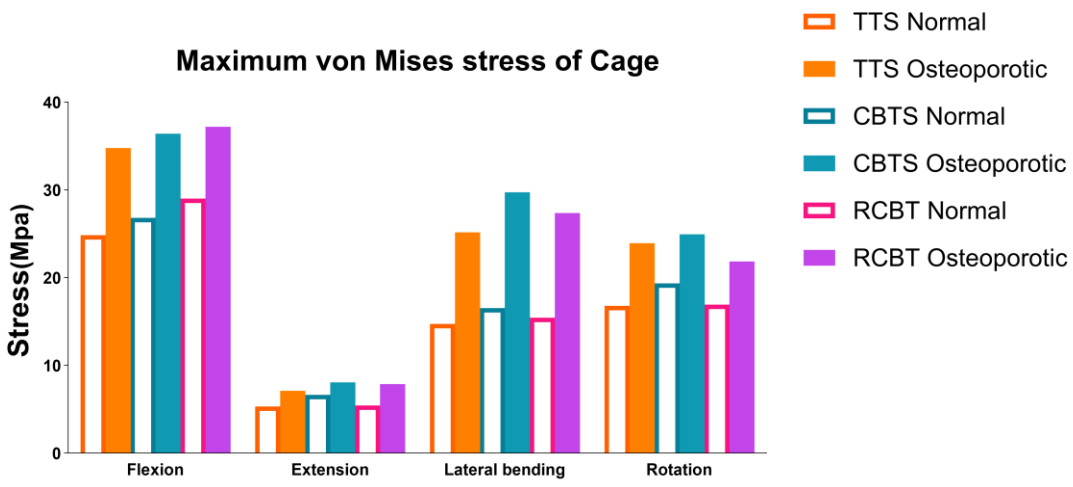


Figure 7. Cage stress under normal and osteoporotic conditions.

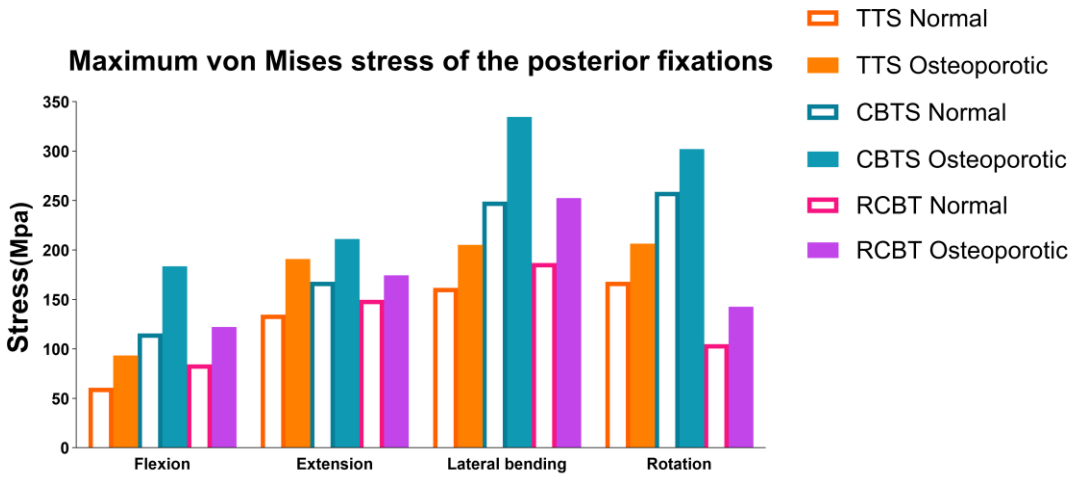
Legend: Maximum von Mises stress of the interbody cage in the TT–TT, CBT–CBT, and CBT–RCBT models under normal and osteoporotic conditions. For consistency with the terminology used in the main text, the figure labels TTS, CBTS, and RCBT correspond to TT-TT, CBT-CBT, and CBT-RCBT, respectively.



685

686 **Figure 8.** Posterior fixation stress under normal and osteoporotic conditions.

687 **Legend:** Maximum von Mises stress of the posterior screw–rod system in the TT–TT,
688 CBT–CBT, and CBT–RCBT models under normal and osteoporotic conditions. For
689 consistency with the terminology used in the main text, the figure labels TTS, CBTS, and
690 RCBT correspond to TT-TT, CBT-CBT, and CBT-RCBT, respectively.



691

692 **Figure 9**. Von Mises stress contours of posterior fixation under osteoporotic conditions.

693 **Legend:** Stress contour plots of the three posterior fixation systems under osteoporotic
694 conditions. High-stress regions were mainly concentrated at the screw head–rod junction
695 and the screw neck/proximal thread region. For consistency with the terminology used in

the main text, the figure labels TTS, CBTS, and RCBT correspond to TT–TT, CBT–CBT, and CBT–RCBT, respectively.

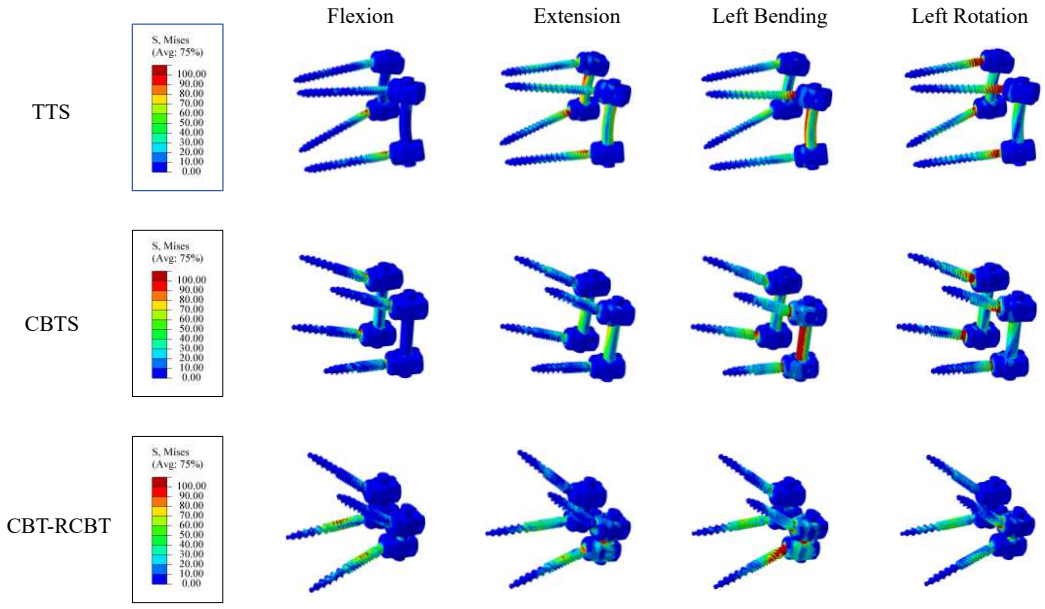


Figure 10. L3/4 disc stress under normal and osteoporotic conditions.

Legend: Stress distribution and mean von Mises stress of the superior adjacent intervertebral disc (L3/4) in the TT–TT, CBT–CBT, and CBT–RCBT models under normal and osteoporotic conditions. For consistency with the terminology used in the main text, the figure labels TTS, CBTS, and RCBT correspond to TT‑TT, CBT‑CBT, and CBT‑RCBT, respectively.

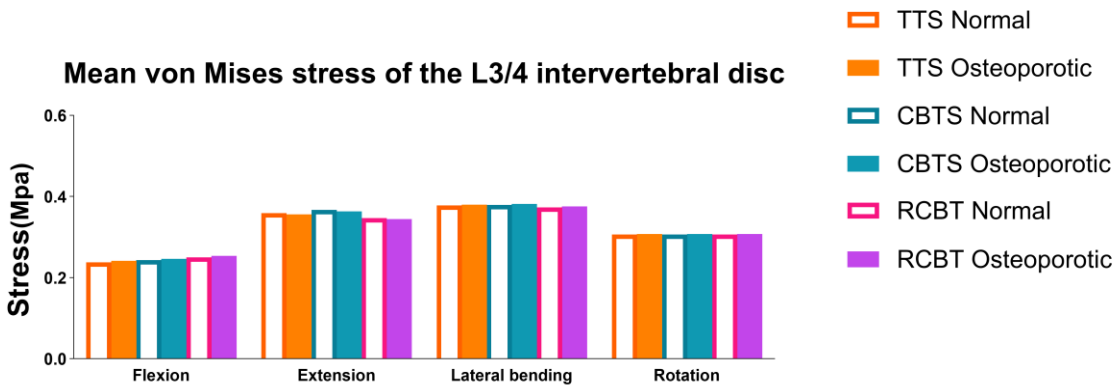


Figure 11. L5/S1 disc stress under normal and osteoporotic conditions.

Legend: Stress distribution and mean von Mises stress of the inferior adjacent intervertebral disc (L5/S1) in the TT–TT, CBT–CBT, and CBT–RCBT models under normal and osteoporotic conditions. For consistency with the terminology used in the main text, the figure labels TTS, CBTS, and RCBT correspond to TT‑TT, CBT‑CBT, and CBT‑RCBT, respectively.

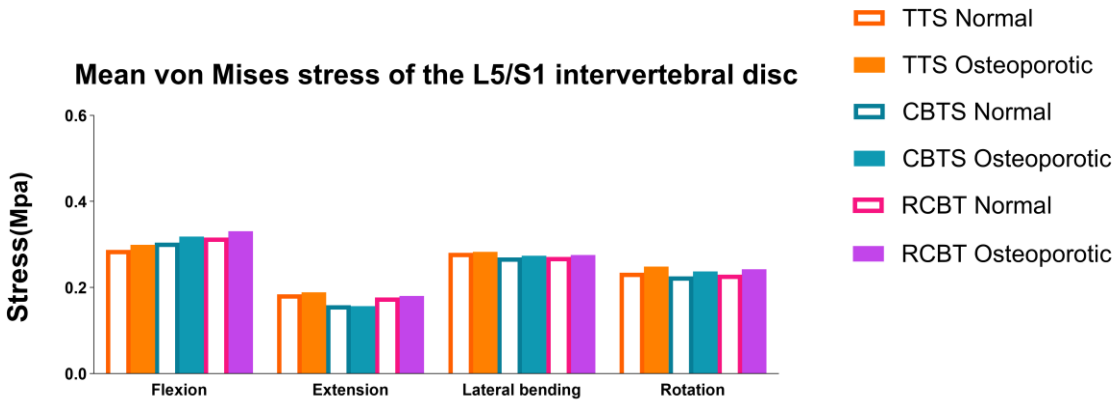


Figure 12. Posterior exposure requirement among the three fixation constructs.

Legend: (A) Bilateral traditional-trajectory pedicle screw fixation (TT–TT). (B) Bilateral cortical bone trajectory screw fixation (CBT–CBT). (C) Hybrid fixation using cranially directed CBT and caudally directed reverse CBT (CBT–RCBT). Posterior exposure

requirement was quantified from standardized posterior-view projections and normalized to the TT–TT construct.

